USE OF AIRBORNE SAR INTERFEROMETRY FOR MONITORING DEFORMATION OF LARGE-SCALE MAN-MADE FEATURES

Scott Hensley[*], *Howard Zebker*[†], *Cathleen Jones*[*], *Thierry Michel*[*], *Ron Muellerschoen*[*], *Bruce Chapman*[*]
[*] Jet Propulsion Laboratory, California Institute of Technology, 4800 Oak Grove Drive, Pasadena, CA 91109
Email: scott.hensley@jpl.nasa.gov
[†]Stanford University, Palo Alto, CA 94305

ABSTRACT

Monitoring the deformation of large scale man-made structures is of vital importance for avoiding catastrophic loss of infrastructure and life. Many structures that require monitoring may span distances from a kilometer, e.g. dams and bridges, to many tens of kilometers, e.g. dikes and levies. First signs of deterioration in these structures can manifest themselves as subtle deformations that may be localized to only a small fraction of the total structure. As the deterioration progresses from initial indications of damage where the magnitude of deformation is millimeters occurring over fairly long times scales of months to a year to more serious levels of deformation indicative of imminent failure of centimeters in the span of hours to days. The magnitude of the deformations, the large range of relevant times scales and the sizes of the structures present a considerable challenge to accurate monitoring of these signatures. Radar interferometry has proven to be an extremely reliable means of measuring subtle deformations of both natural and man-made structures with accuracies that span the levels of deformation that require monitoring. The large array of currently operating and planned earth observing orbiting radars coupled with advanced processing schemes such as permanent scatterer techniques can play a major role in this regard. Nevertheless, airborne radar interferometric sensors with higher resolution and more flexible repeat intervals and flight geometries can improve the detectability and provide a level of targeted response not possible with satellite systems. This paper will illustrate the value of airborne sensors to monitoring deformation using examples from the NASA/JPL UAVSAR radar instrument.

1. INTRODUCTION

A robust monitoring capability for monitoring large scale deformation of man-made structures should have the following elements:

- The sensitivity to measure the millimeter level and greater deformation of the structures.
- The ability to measure deformations that are occurring on times scales from hours to a year.
- Have sufficient spatial resolution to detect localized defects in the structure and diagnose its implications.
- The ability to monitor deformation occurring over spatial scales ranging from a kilometer to tens of kilometers.
- The ability to configure the monitoring scenario for both background monitoring and for critical situations.

Such a capability places considerable demands on any monitoring system and thus it likely to be composed of multiple observing sensors that are suited to the various aspects of measuring the deformation on large scale man-made structures.

Over the last 3 decades radar interferometry has proven to be a valuable technique for measuring both naturally occurring and anthropogenically induced deformation. Most of these measurements have been made with spaceborne systems that have repeat intervals of a month or greater and support deformation products with spatial resolution of 50 m or more.[1] With the advent of permanent scatterer processing techniques these sensors have been used to monitor deformation from a large array of natural and man-made structures including large scale structures such as dams and dikes, [7], [6], [3], and [2]. An appropriately configured airborne radar interferometric sensor could make similar measurements while meeting many of the elements of a robust monitoring capability defined previously. Extending radar ineterferometric deformation observations from spaceborne to airborne systems is made difficult by the irregular flight trajectories flown by aircraft systems and the variation in the aircraft attitude angles from pass to pass. Recently, NASA/JPL implemented an airborne L-band radar system, called UAVSAR, designed specifically for repeat pass radar interferometric observations. The aim of this paper is to illustrate, by using data from the UAVSAR system, that an airborne system could prove extremely useful for measuring deformation from large scale man-made structures. The remainder of the paper is organized as follows: Section 2 provides a quick overview of radar interferometric deformation measurements, Section 3 provides an overview of the UAVSAR instrument, Section 4 provides a description of the data processing, Section 5 shows some examples of deformation measurements made using the UAVSAR instrument and finally some conclusions are given in Section 6.

2. DEFORMATION INTERFEROMETRY

Differential radar interferometry is routinely used to measure millimeter level surface deformation by acquiring radar observations on temporally separated images spanning a time

[1]A notable exception is the German TERRASAR-X system launched in 2007 with a repeat interval of 11 days and modes with resolutions of less than a meter.

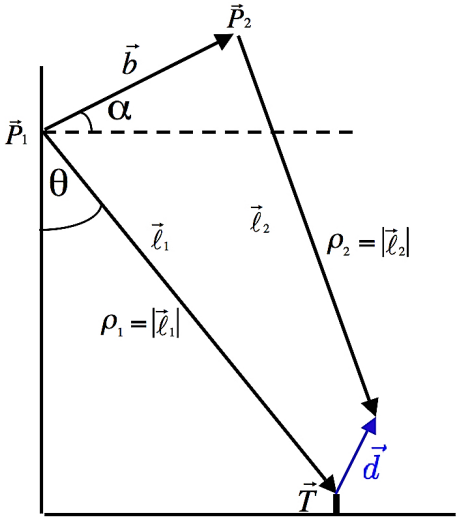

Fig. 1. *Diagram of the repeat pass imaging geometry for deformation measurement.*

interval over which the surface was deforming. The interferometric phase measurement couples information concerning the line-of-sight surface deformation as well as a topographic signature that must be removed from the data before the deformation signal can be extracted. Additionally, the interferometric phase is corrupted by changes in the imaging environment between observations; in particular, changes in the troposphere and ionosphere can induce multi-centimeter level distortions to the deformation signal at spatial scales from a kilometer to hundreds of kilometers.

The inteferometric phase for repeat pass observations is given by

$$\phi = \frac{4\pi}{\lambda}(\rho_2 - \rho_1) \tag{1}$$

where ρ_1 and ρ_2 are the ranges from the antenna phase center of radar to a resolution element for two observations and λ is the radar wavelength. Letting $\vec{\ell}_i, i = 1,2$ be the look vectors from the radar phase center locations, $\vec{P}_i, i = 1,2$ to the resolution element located at, $\vec{T}$, then Equation 1 can be rewritten as

$$\phi = \frac{4\pi}{\lambda}\left(|\vec{\ell}_2| - |\vec{\ell}_1|\right) = \frac{4\pi}{\lambda}\left(\langle\vec{\ell}_2, \vec{\ell}_2\rangle^{\frac{1}{2}} - \rho_1\right) \tag{2}$$

where $\vec{\ell}_i = \vec{T} - \vec{P}_i$ and $\rho_i = |\vec{\ell}_i|$. If $\vec{d}$ denotes the vector surface deformation between observations and $\vec{b} = \vec{P}_2 - \vec{P}_1$, is the baseline vector, as shown in Figure 1, then $\vec{\ell}_2$ can be expressed in terms of $\vec{b}$, $\vec{\ell}_1$ and $\vec{d}$ as

$$\vec{\ell}_2 = \vec{\ell}_1 + \vec{d} - \vec{b}. \tag{3}$$

Substituting Equation 3 into Equation 2 yields

$$\begin{aligned}\phi &= \frac{4\pi}{\lambda}\rho_1\left[\left(1 + \frac{2\left(\langle\hat{\ell}_1, \vec{d}\rangle - \langle\hat{\ell}_1, \vec{b}\rangle - \langle\hat{d}, \vec{b}\rangle\right)}{\rho_1}\right.\right. \\ &+ \left.\left.\frac{b^2 + d^2}{\rho_1^2}\right)^{\frac{1}{2}} - 1\right]\end{aligned} \tag{4}$$

where $\hat{\ell}_1 = \frac{\vec{\ell}_1}{\rho_1}$. Taylor expanding Equation 5 to first order and assuming $|\vec{b}| << \rho_1$, $|\vec{d}| << \rho_1$ and $|\langle\vec{b}, \vec{d}\rangle| << \rho_1$ yields the basic repeat pass deformation equation

$$\phi = \frac{4\pi}{\lambda}\left(\langle\vec{d}, \hat{\ell}\rangle - \langle\vec{b}, \hat{\ell}\rangle\right) \tag{5}$$

where the subscript 1 is dropped for ease of notation. The first term in Equation 5 is the projection of the deformation vector onto the line-of-sight vector and the second term is the topographic contribution to the interferometric phase. Eliminating the second term requires either *a priori* topographic data, e.g., a digital elevation model (DEM), or using multiple pass techniques to generate the topographic information. For the purposes of this analysis it is assumed a DEM is available with known height accuracy.

The topographic term can be decomposed into two terms by writing the look vector as the sum of a vector pointing to some reference surface plus a vector pointing from the reference surface to the actual imaged resolution element. Writing $\hat{\ell} = \hat{\ell}_o + \frac{\Delta\vec{\ell}}{\rho}$ and substituting into the second term in Equation 5 yields the follwoing expression for the topographic phase, ϕ_t,

$$\phi_t = -\frac{4\pi}{\lambda}\langle\vec{b}, \hat{\ell}\rangle = -\frac{4\pi}{\lambda}\langle\vec{b}, \hat{\ell}_o\rangle - \frac{4\pi}{\lambda}\langle\vec{b}, \frac{\Delta\vec{\ell}}{\rho}\rangle. \tag{6}$$

Since $\vec{\ell}$ and $\vec{\ell}_o$ have the same range the vectors $\Delta\vec{\ell}$ and $\hat{\ell}$ are perpendicular and hence $\Delta\vec{\ell}$ is parallel to a unit vector perpendicular to the line-of-sight vector denoted $\hat{\ell}_\perp$. The length of $\Delta\vec{\ell}$ is simply the height of the terrain, h_t, divided by the sine of the look angle, θ. Thus, the topographic phase term can be written as

$$\begin{aligned}\phi_t &= -\frac{4\pi}{\lambda}\langle\vec{b}, \hat{\ell}_o\rangle - \frac{4\pi}{\lambda\rho\sin\theta}\langle\vec{b}, \hat{\ell}_\perp\rangle h_t \\ &= -\frac{4\pi}{\lambda}\langle\vec{b}, \hat{\ell}_o\rangle - \frac{4\pi b_\perp}{\lambda\rho\sin\theta}h_t\end{aligned} \tag{7}$$

which is readily computed from the imaging geometry, knowledge of the baseline and the elevation of the resolution element. After eliminating the topographic phase the resulting phase is only a function of the projection of the deformation vector onto the line-of-sight, d_{los}. Thus the line-of-sight deformation is related to the topographically corrected interferometric phase, $\tilde{\phi}$, by

$$\Delta\rho \approx d_{los} = \langle\vec{d}, \hat{\ell}\rangle = \frac{\lambda}{4\pi}\tilde{\phi}. \tag{8}$$

3. UAVSAR OVERVIEW

Making robust repeat-pass radar interferometric measurements (RPI) at L-band to measure both natural and anthropogenically induced deformation of the Earth's surface from an airborne platform presents difficulties not found in spaceborne observations due to the above mentioned navigation and pointing constraints. The UAVSAR radar is designed from the beginning as a miniaturized polarimetric L-band radar for repeat-pass and single-pass interferometry with options for along-track interferometry and additional frequencies of operation. The radar has been initially deployed on the NASA

Fig. 2. *Modified NASA Gulfstream III in early flight tests with the UAVSAR pod attached to the underside of the aircraft. Photo courtesy of NASA Dryden Flight Research Center.*

Gulfstream III aircraft and porting to the Global Hawk UAV is presently under development. Figure 2 shows the instrument pod attached to the underside of the NASA Gulfstream III during early flight testing of the aircraft modifications. Key measurements the system has been designed to make in support of various NASA science programs include:

- Precision crustal deformation for monitoring earthquakes both during and after a seismic event, for monitoring volcanic activity and for monitoring human-induced surface change such as subsidence induced by oil or water withdrawal, or other displacements of the surface from human activities.
- Polarimetric interferometry, which can provide measurements of forest structure and sub-canopy topography.
- Polarimetric tomography, mapping in detail the vertical structure of a vegetated area.

Robust repeat-pass radar interferometric measurement imposes two observational constraints on the UAVSAR radar and system. First, it is necessary that on repeat observations the aircraft fly within a specified distance of its previous flight trajectory. UAVSAR has a science-derived requirement for flight track repeatability of 10 m, hence NASA Dryden has modified the NASA Gulfstream III to include a Precision Autopilot capability [5] to control aircraft position. The precision autopilot uses input from the real-time DGPS to generate signals that are used to drive the aircraft's ILS landing system. With well over 40 flights conducted to date, the Precision Autopilot has been shown to exceed its requirements and normally flies within a 5 m tube. Secondly, it is also essential that the antenna look directions are identical within a fraction of the beamwidth. Because the wind can be substantially different at different times, even if the platform is capable of accurately repeating the desired track, the yaw angle of the aircraft can vary widely on different tracks due to different wind conditions aloft. UAVSAR thus employs an electronically steered flush mounted antenna that is pointed in the desired direction based on real-time attitude angle measurements. Based on the science objectives and the platform characteristics, the key parameters of the radar design are given in Table I. In the following sections, we briefly highlight the basic design element of the UAVSAR radar and present a few examples of deformation measured using the UAVSAR instrument.

TABLE I

RADAR PARAMETERS

Parameter	Value
Frequency	1.26 GHz (.2379 m)
Bandwidth	80 MHz
Pulse Duration	5-50 μs
Polarization	Quad Polarization
Range Swath	16 km
Look Angle Range	$25^\circ - 65^\circ$
Transmit Power	3.1 kW
Antenna Size	0.5m $\times$ 1.6 m
Operating Altitude Range	2000-18000 m
Ground Speed Range	100-250 m/s

The radar has been designed to minimize the number of interfaces with the aircraft for improved portability. The aircraft provides 28 V DC power to the radar via the Power Distribution Unit (PDU), which is also responsible for maintaining the thermal environment in the pod, and the radar provides its real-time DGPS position data to the aircraft for use by the Precision Autopilot. Waypoints for the desired flight paths are generated prior to flight by the Flight Planning Subsystem (FPS) and loaded into the Precision Autopilot and into the radar's Automatic Radar Controller (ARC) along with radar command information for each waypoint. The ARC is the main control computer for the radar and controls all major functions of the radar during flight. It is designed to operate in a fully autonomous mode or to accept commands from the Radar Operator Workstation (ROW) either through an ethernet connection on crewed platforms or through an Iridium modem for uncrewed platforms. The Control and Timing Unit (CTU) controls the timing of all the transmit and receive events in the radar timeline and thus interacts with many of the radar digital and radio frequency (RF) electronics. The active array antenna consists of 24 130 W L-band Transmit/Receive (TR) modules that feed 48 radiating elements within the 0.5 m by 1.5 m array.

4. DATA PROCESSING OVERVIEW

Generation of image and science data products follows motion processing that consists of blending data from the inertial navigation unit (INU) and differential GPS data that has been processed on the ground for maximal accuracy. After the motion processing step is completed for a repeat-pass pair of images, a subsequent motion alignment algorithm is employed to determine proper processing parameters for the science data so that the imagery will be co-aligned in both the along-track and cross-track directions. Also, a common coordinate system and reference path based on the two trajectories is selected. Data for both passes are then processed through the image formation processor to generate single look complex (SLC) imagery. If the ephemeris knowledge were perfect then the two images would be co-registered precisely. However, even with the best post processing of the DGPS data, the expected relative position accuracy between the two passes

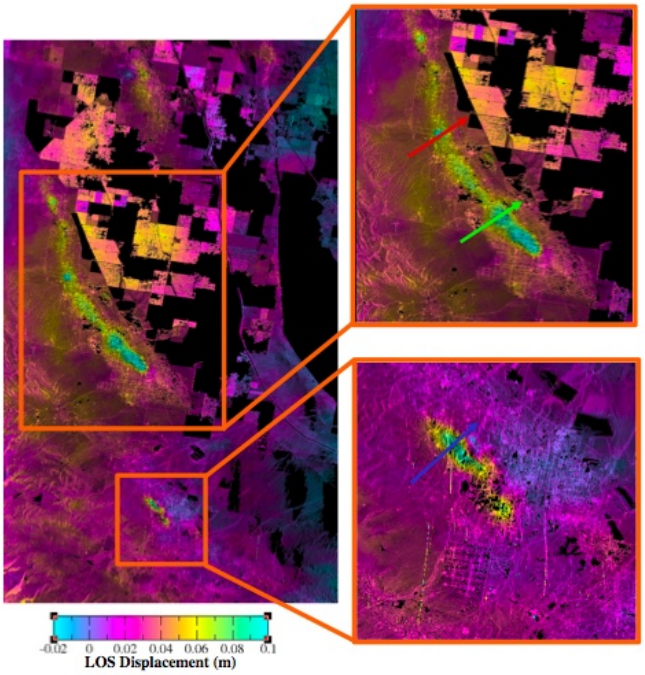

Fig. 4. *Deformation due to oil pumping near Lost Hills California.*

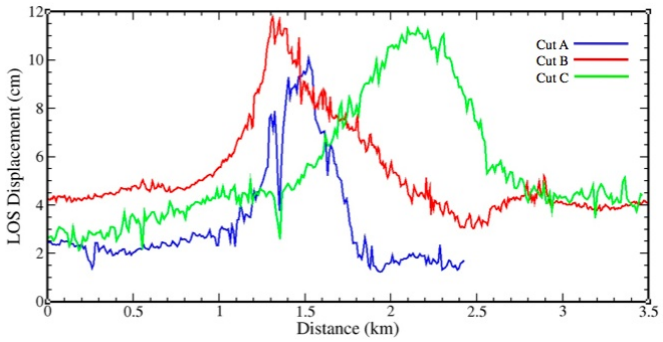

Fig. 5. *Plots of the displacement along several transects highlighted by arrows in Figure 4.*

is on the order of 2-3 cm, an order of magnitude or more larger than the required accuracy to achieve the fraction of a pixel offset that is required for interferometric applications. To achieve improved alignment, the relative position data, called the baseline, is refined based on the SLC images themselves. Several methods exist for recovering residual motion. These differ in implementation and accuracy, however, the basic idea is to use the mis-registration information between the SLC images to derive a baseline correction as discussed in [4]. After the residual baseline is estimated the improved ephemeris is used to reprocess the data. The procedure may be repeated until the two images are co-registered with sufficient accuracy. Figure 3 shows the RTI baseline for two passes collected a week apart over the San Joaquin Valley in California and the residual motion estimated from the SLC image mis-registration as described previously.

An interferogram is formed by multiplying the complex value of a pixel in one image by the complex conjugate of the corresponding pixel in the second image of the interferometric pair. It is the phase of the complex value in the interferogram that contains the deformation signal. However, the interferometric phase measurement suffers from two complicating factors that must be addressed before the deformation signal can be extracted. First, the interferometric phase encodes not only the surface deformation signal, but also a measurement of the surface topography whenever the baseline is non-zero. With the advanced terrain dependent motion compensation employed during image formation, the topographic fringes are automatically removed when interferogram is formed. Also, the interferometric phase is only measured modulo 2π, which represents one half wavelength (12 cm) of surface deformation. Since the deformation signal can be many multiples of 2π, a two dimensional phase unwrapping procedure is applied to get an unambiguous deformation measurement. After geocoding data from multiple repeat-passes, they are combined to reduce thermal and atmospheric noise, or, if the data are collected from multiple vantages, we reconstruct the three dimensional deformation vector. A single interferometric measurement is only sensitive to deformation in the line-of-sight direction.

5. EXAMPLES

5.1 *Oil Pumping at Lost Hills, CA*

UAVSAR collected two passes of 74 km in length over Lost Hills, CA on May 6 and July 25 of 2008 from an altitude of 12.5 km. This area is known to be undergoing surface deformation due to oil pumping based on satellite radar interferometric measurements and GPS measurement [8]. The area is mostly agricultural interspersed with light urban development and thus many areas remain highly correlated for large temporal baselines at L-band. The two passes were separated by eighty days and were processed as described in Section 4. Obvious from the radar interferogram are two areas undergoing surface deformation centered over light urban areas. Figure 4 shows the line-of-sight displacement obtained from the unwrapped interferometric phase with a spatial resolution of about 7 m (36 looks). L-band has good correlation over the urban development and in some fallow agricultural regions. The maximal displacement is about 7 cm corresponding to a deformation rate of about 0.88 $\frac{mm}{day}$. Figure 5 shows the plots of the displacement along selected transects highlighted in Figure 4 which are about 3 km in length. Note the asymmetric nature of the displacement profiles along cuts A and B which would be difficult to discern in satellite imagery due to their coarser resolution.

5.2 *Landslide Detection*

Repeat-pass tracks about 160 km in length were collected and processed over the San Andreas Fault near Parkfield, CA with temporal baselines of 31 and 80 days which were collected on April 28, May 29 and July 24 of 2008. This is area of interest because of known creep on the San Andreas Fault near Parkfield. Of particular interest are the small landslides of approximately 2 kilometers in size detected in both the 31 and 80 day repeat passes. Figures 6 and 7 show the 31 and 80 day

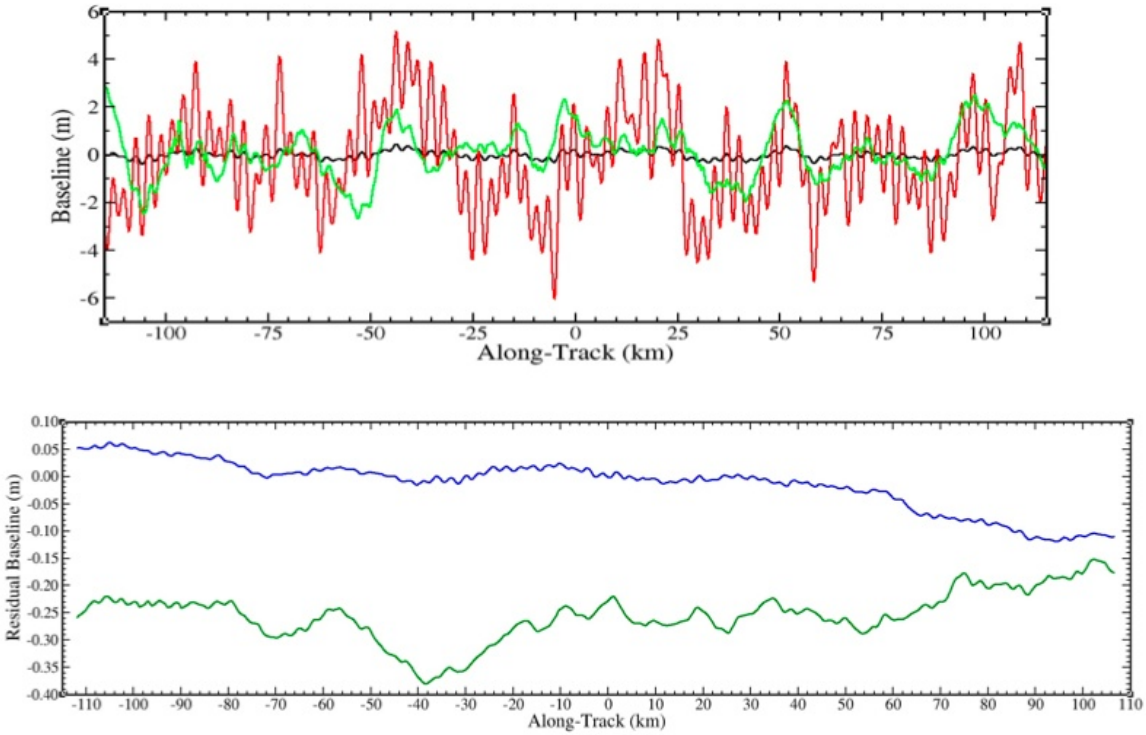

Fig. 3. *Repeat pass baseline estimated directly from blended INU and DGPS data and the correction to the baseline estimated from offset data. In the upper plot black is the along-track component of the baseline, red is the cross-track component and green is the vertical component. In the lower plot blue is the cross-track component of the residual baseline and green is the vertical component.*

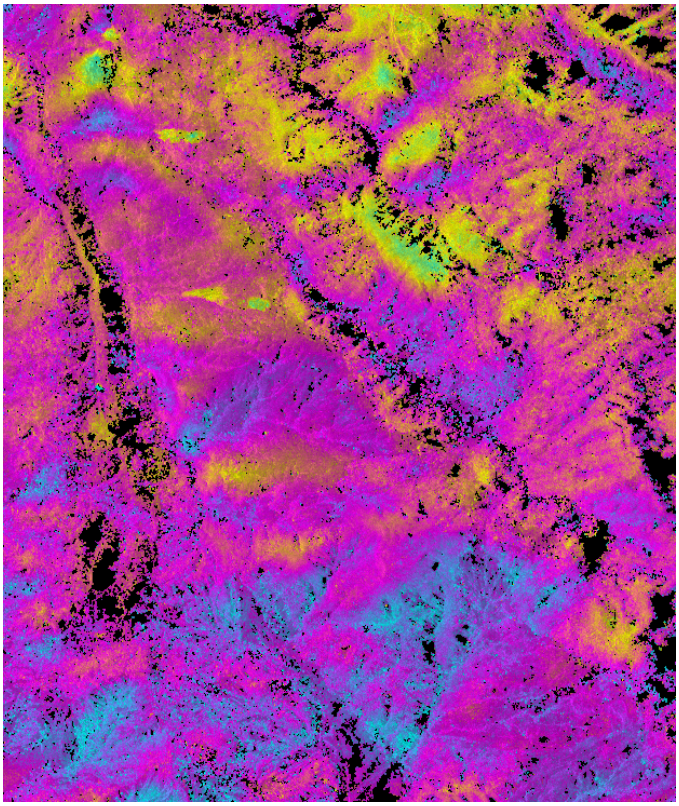

Fig. 6. *Line-of-sight displacement observed after a 31 day repeat for an area containing the three landslides that are approximately 2 km in length.*

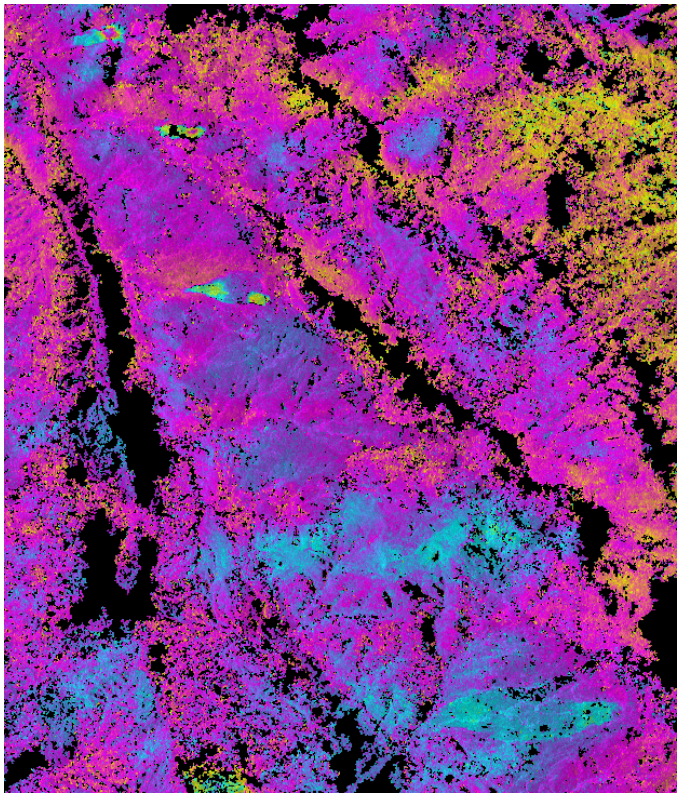

Fig. 7. *Line-of-sight displacement observed after a 80 day repeat for an area containing the three landslides that are approximately 2 km in length.*

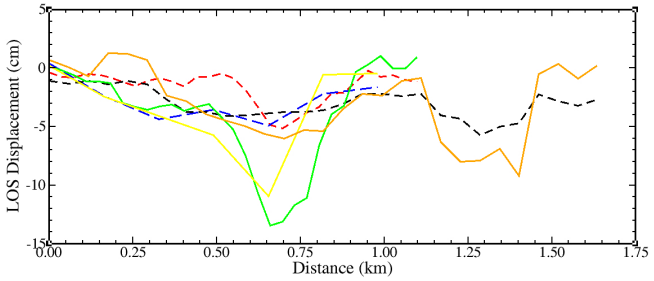

Fig. 8. *Plots of the line-of-sight displacement through transects oriented along the 3 landslides shown in Figures 6 and 7.*

repeat pass data of an approximately 6 by 8 km portion of the unwrapped phase converted to line-of-sight displacements over a region of the 160 km long swath showing three landslides. Displacement measurements have a spatial resolution of about 7 m with 36 looks. Transects along the three landslides for the 31 day repeat (dotted lines) and 80 day repeat (solid lines) that are about 2 km in length are shown in Figure 8. Note the line-of-sight displacements for the 80 day repeat compared to the 31 day repeat show continued movement on the landslides. The accuracy of the line-of-sight displacement measurements is 2-3 millimeters with a spatial of 7 m resolution.

6. CONCLUSION

This paper has presents the desired characteristics of a metrology system for measuring deformation on large scale man-made structures. The wide area and the potentially localized nature of deleterious deformation with a variety of temporal scales from hours to a year on these structures necessitate a very capable observing system. Herein it is suggested that an appropriately configured airborne repeat pass radar interferometric observing capability could meet a number of these demanding metrology requirements and when when coupled with other measurements, e.g., GPS, might be a viable component of an observing system for a variety of structures. Two examples based on pumping of oil at Lost Hills and landslides with spatial extent on the order of a couple of kilometers and 1- 8 cm of deformation and landslide deformation with several centimeters of deformation were used to illustrate the potential utility of such a system to large scale man-made structures. Currently, Cathleen Jones, one of the co-authors, is leading a study using UAVSAR to monitor levee deformation in the Sacramento Delta of California, which will be reported on at a later date. Additional information and images can be found at the UAVSAR website [1].

ACKNOWLEDGMENT

This research was conducted at the Jet Propulsion Laboratory, California Institute of Technology, under contract with the National Aeronautics and Space Administration.

Reference herein to any specific commercial product, process, or service by trade name, trademark, manufacturer, or otherwise, does not constitute or imply its endorsement by the United States Government or the Jet Propulsion Laboratory, California Institute of Technology.

References

[1] http://uavsar.jpl.nasa.gov.

[2] J. Groot. River dike deformation measurement with airborne sar. *Geoscience and Remote Sensing Letters, IEEE*, 1(2):94–97, April 2004.

[3] R.F. Hanssen and F.J. van Leijen. Monitoring water defense structures using radar interferometry. *Radar Conference, 2008. RADAR '08. IEEE*, pages 1–4, May 2008.

[4] S. Hensley, T. Michel, M. Simard, C. Jones, R. Muellerschoen, C. Le, H. Zebker, and B. Chapman. Residual motion estimation for uavsar: Implications of an electronically scanned array. Proceedings of Radarcon 2008, 2008.

[5] James Lee, Brian Strovers, and Victor Lin. C-20A/GIII Precision Autopilot development in support of NASAs UAVSAR program. In *Proceeding of the NASA Science Technology Conference 2007*, Greenbelt, Maryland, June 2007. NASA.

[6] D. Perissin, C. Prati, F. Rocca, and Teng Wang. Psinsar analysis over the three gorges dam and urban areas in china. *Urban Remote Sensing Event, 2009 Joint*, pages 1–5, 2009.

[7] D. Tarchi, H. Rudolf, G. Luzi, L. Chiarantini, P. Coppo, and A.J. Sieber. Sar interferometry for structural changes detection: a demonstration test on a dam. *Geoscience and Remote Sensing Symposium, 1999. IGARSS '99 Proceedings. IEEE 1999 Internationa*, 3:1522–152, 1999.

[8] M. Van der Kooij and D. Mayer. The application of satellite radar interferometry to subsidence monitoring in the belridge and lost hills fields, california. volume 1 of *Geoscience and Remote Sensing Symposium, 2002. IGARSS '02. 2002 IEEE International*, pages 201– 202, 2002.